Materials Today Bio 15 (2022) 100335

Contents lists available at ScienceDirect

Materials Today Bio

journal homepage: www.journals.elsevier.com/materials-today-bio

A role for nuclear stretching and NPCs changes in the cytoplasmic-nuclear trafficking of YAP: An experimental and numerical modelling approach

Stefania Saporito [a,b], Carlo F. Natale [b], Costantino Menna [c], Paolo Antonio Netti [a,b,d], Maurizio Ventre [a,b,d,*]

[a] Department of Chemical, Materials and Industrial Production Engineering, University of Naples Federico II, Italy
[b] Center for Advanced Biomaterials for Healthcare@CRIB, Istituto Italiano Di Tecnologia, Italy
[c] Department of Structures for Engineering and Architecture, University of Naples Federico II, Italy
[d] Interdisciplinary Research Center on Biomaterials (CRIB), University of Naples Federico II, Italy

ARTICLE INFO

Keywords:
Mechanobiology
Nuclear pores
Micropatterning
Finite element models
Stem cells

ABSTRACT

Mechanical forces, acting on eukaryotic cells, are responsible for cell shape, cell proliferation, cell polarity, and cell differentiation thanks to two cells abilities known as mechanosensing and mechanotransduction. Mechanosensing consists of the ability of a cell to sense mechanical cues, while mechanotransduction is the capacity of a cell to respond to these signals by translating mechanical stimuli into biochemical ones. These signals propagate from the extracellular matrix to the nucleus with different well known physical connections, but how the mechanical signals are transduced into biochemical ones remains an open challenge. Recent findings showed that the cell-generated forces affect the translocation of transcription factors (TFs) from the cytoplasm to the nucleus. This mechanism is affected by the features of nuclear pore complexes. Owing to the complex patterns of strains and stresses of the nuclear envelope caused by cytoskeletal forces, it is likely that the morphology of NPC changes as cytoskeleton assemblies' change. This may ultimately affect molecular transport through the nucleus, hence altering cell functions. Among the various TFs, Yes-associated protein (YAP), which is typically involved in cell proliferation, survival, and differentiation, is able to activate specific pathways when entrapped into the cell nucleus. Here, starting from experimental results, we develop a multiscale finite element (FE) model aimed to simulate the macroscopic cell spreading and consequent changes in the cell mechanical behaviour to be related to the NPCs changes and YAP nuclear transport.

1. Introduction

Mechanosensing and mechanotransduction are two mechanisms by which eukaryotic cells can perceive and transform mechanical stimuli into biochemical signals [1,2].

Cell mechanoregulation has attracted a strong interest inasmuch the extracellular and intracellular mechanical forces appear to regulate the nuclear import of transcriptional activators of genes that are responsible for the regulation of many aspects of cellular behaviour such as cell shape, cell proliferation, cell polarity and cell differentiation. Furthermore, in pathological conditions, such as cancers or neurodegenerative diseases, mechanosensing and mechanotransduction pathways may differ from those of normal cells [1,3].

Cells perceive their mechanical microenvironment through discrete molecular complexes attached to the extracellular matrix (ECM), called focal adhesions (FAs), formed by membrane-spanning integrins and other proteins like kinase, talin and vinculin [4–6]. FAs create a direct communication between the ECM and the cytoskeleton of cells. Furthermore, the cytoskeleton and the nuclear envelope (NE) are physically connected through the LINC complex, which provides a mechanism for transmitting extracellular forces to the nucleus through the cytoskeleton. This coupling is established with specific proteins of the outer nuclear membrane (Nesprin 1 and 2), which bind to both cytoskeletal filaments and inner nuclear membrane proteins (SUN 1 and 2). These are connected to the lamins of the nuclear lamina and to other proteins of the nuclear membrane, which, in turn, interact with the nuclear DNA structure [6]. In addition to this physical connection, the actin cap, composed of thick, parallel, and contractile actomyosin filament bundles running on the nucleus upper surface [4,5], is able to directly exert compressive forces to the nucleus, thus deforming its membrane and displacing its matter. Even if the physical connections between ECM, cytoskeleton and nucleus are well known, the mechanism underpinning

* Corresponding author. Department of Chemical, Materials and Industrial Production Engineering, University of Naples Federico II, Italy.
E-mail address: maventre@unina.it (M. Ventre).

https://doi.org/10.1016/j.mtbio.2022.100335
Received 22 March 2022; Received in revised form 27 May 2022; Accepted 16 June 2022
Available online 22 June 2022

the transduction of mechanical insults into precise biochemical signals remains largely unknown.

Recent findings demonstrated that cell-generated forces affect the translocation of transcription factors (TFs) from the cytoplasm to the nucleus through diverse mechanisms [7–9]. However, the transport of all macromolecules between the nucleus and the cytoplasm is mediated by the nuclear pore complexes (NPCs), specialized nano-pore structures that are distributed along the NE, which separates the nucleoplasmic environment from the cytoplasmic one [1,10,40]. Each NPC is a multiprotein structure composed of three coaxial 8-fold rotational symmetric rings; in particular, the main rings are: spoke ring (SR), cytoplasmic ring (CR) and nuclear ring (NR). A specific filament structure known as nuclear basket grows from the nuclear ring and ends in a smaller one called the distal ring (DR) [1,10–12]. The NPCs work as selective filters for the import-export transport of molecules between the nucleus and the cytoplasm. In fact, under an undeformed cell configuration, the molecules can pass through a diffusive pathway if they have a molecular weight from 40 to 60 kDa [1,10,11,13–17]. Conversely, the molecules with a higher molecular weight than the cut-off value can move only through a facilitated transport mediated by specific cargos [1,10,11,13–17].

Owing to the complex patterns of strain and stresses of the nuclear envelope caused by cytoskeletal forces, it is likely that the morphology of NPC changes as cytoskeleton assemblies' change. This may ultimately affect molecular transport through the nucleus, hence altering cell functions. In particular, the cytoplasm-nuclear shuttling of TFs has been correlated with the mechanical state of the nucleus [7,11]. Among the various TFs, Yes-associated protein (YAP), which is typically involved in cell proliferation, survival, and differentiation [9], is able to activate specific pathways when entrapped into the cell nucleus, whereas it is inactive into the cytoplasm [9,18]. Interestingly, the molecular weight (65 kDa) of this TF is comparable to the cut-off value of molecular weight for undeformed NPCs, which makes YAP particularly sensitive to mechanical stresses/deformations acting on the nucleus, as a small stretching of pores may determine a switch from active to passive transport [7,11,19,20]. However, the role of the morpho-mechanical features of the nucleus in affecting TFs shuttling via pore stretching has not been thoroughly investigated.

Here we develop a multiscale finite element (FE) model aimed to simulate the macroscopic cell spreading and consequent changes in the cell mechanical behaviour to test the hypothesis on whether the intracellular stresses alter the configuration of NPC hence affecting YAP nuclear transport. The model was supported by an experimental campaign designed to control cell shape and thus the intracellular stress states. In detail, we cultivated Adipose Stem Cells (ASCs) on micropatterned surfaces consisting of adhesive islets in the form of circular and rectangular shapes with the same cell spreading area (1300 μm^2 - small patterns; 5000 μm^2 - large patterns). The FE modelling strategy consisted in the definition of two numerical models representing two different scales of observation: (i) a full 3D non-linear mechanical model (named as "macro-model") that reproduced the stretching/spreading of the whole-cell lying on the substrate and based on a proper experiment-derived displacement field as function of micropattern geometry; and (ii) a specific 2D "periodic meso-model" (hereafter referred to as "meso-model") of the NE subjected to pattern-related displacements derived from the full 3D FE simulations. The meso-models are devoted to assessing the response of the NPCs as a function of the variable cell spreading/confinement conditions.

2. Materials and Method

2.1. Experimental part

2.1.1. Substrate fabrication and functionalization

Fabrication of culture substrates with specific microscopic features was made using the UV-deep light micropatterning technique according with the protocol developed by *Azioune* et al. [21]. Briefly, glass coverslips were washed in 70% ethanol for 10 min and dried. Then, they were first activated by exposure to O_2 plasma (PFEIFFER VACUUM Single-Gauge – CESAR RF Power Generator) for 1 min and incubated for 1 h with 0.1 mg mL^{-1} poly-L-lysine-g-poly(ethyleneglycol) (PLL-(20)-g[3.5]-PEG(2); 4DCell, Montreuil, France) in 10 mM HEPES at pH 7.3 for passivation. After washing with distilled water, the treated surfaces were illuminated with deep UV light (ProCleaner Plus, BioForce Nanosciences, Virginia Beach, VA, United States) through a chromium synthetic quartz photomask (4DCell), possessing the desired micropattern feature (Fig. S1), for 3 min to selectively burn desired PLL-g-PEG regions.

The mask has a square shape, and it is divided in four different square sub-regions: C1, C2, R1 and R2 (Fig. S1). Each adhesive island has a distance from the others of 50 μm that should be enough to avoid the jump of a cell from an adhesive island to the closest one and the paracrine communication between them.

2.1.2. Cell culture and cell seeding

ASC52telo, hTERT immortalized adipose derived Mesenchymal Stem Cells (hTERT; ATCC) in passages four to eight were cultured in Mesenchymal Stem Cell Basal Medium (ATCC) supplemented with mesenchymal stem cell growth kit for adipose and umbilical-derived MSCs – Low Serum (ATCC) at 37 °C in a humidified atmosphere of 95% air and 5% CO_2; the culture medium was changed every 2 days. After 3 days of culture, cells were detached with trypsin (Gibco, Thermo Fisher Scientific, Waltham, MA, USA) and seeded on all patterned substrates at a density of 4000 cells/cm^2. Prior to cell seeding, all patterned, and reference substrates were incubated for 1 h with 50 μg/mL fibronectin solution (Sigma-Aldrich, St. Louis, MO, USA) at room temperature. The reference substrates are referred to analyse the cells into undeformed configuration. This means that, after 1 h from cell seeding, three different samples have been fixed to know the cellular and nuclear dimension in the initial configuration.

2.1.3. Cell fixation and immunostaining

Cells cultured on all patterned substrates were fixed at 1 h (reference substrates), 24 h and 48 h after seeding with 4% paraformaldehyde (Alfa Aesar-Thermo Fisher, Karlsruhe, Germany) in PBS for 15 min. The cells were then permeabilized with 0.1% Triton X-100 (Sigma Aldrich-Merck KGaA, Darmstadt, Germany) in 1x PBS (TPBS). Samples were blocked in 3% bovine serum albumin in PBS (Sigma-Aldrich) for 1 h to avoid non-specific binding. YAP was labelled by incubating samples with an anti-YAP monoclonal antibody (dilution 1:200, Thermo Fisher Scientific – Invitrogen, Table S1) overnight at 4 °C. After incubation, substrates were washed three times with TPBS (3 min per wash) and incubated with Anti-Rabbit IgG (H + L) highly cross-adsorbed secondary, Alexa Fluor 488 (dilution 1:1000; Alexa Fluor ™ Thermo Fisher Scientific, Table S1) for 1 h at 20 °C. Actin filaments were stained by incubating samples with Phalloidin-iFluor 555 reagent (dilution 1:250: ABCAM, Table S1) for 1 h at 20 °C. Nuclei were stained incubating samples with DAPI (4',6-Diamidino-2-Phenylindole, Dihydrochloride, Thermo Fisher Scientific, Table S1) solution (dilution 1:10000) for 15 min. Samples were thoroughly rinsed in PBS and mounted on glass slides by using mounting media (Sigma-Aldrich). Fluorescent images of nuclei, actin bundles and YAP were collected with Confocal Zeiss Axio Observer.Z1 using a 63X objective. Samples were excited at 380 nm (Nuclei), 488 nm (YAPs) and 543 (Actin), and the emissions were collected in the 400–420 nm, 500–530 nm, and 660–690 nm ranges, respectively. Moreover, Z-stacks were acquired with the optimal interval suggested by the software, followed by the application of a maximum intensity algorithm.

2.1.4. Image acquisition and analysis

Area, aspect ratio, major and minor axis of both cells and nuclei were evaluated with the command "Measure" of Fiji. At least 20 confocal digital images at 24 h and at least 10 at 48 h were randomly collected and analysed for each substrate. Cell thickness was assessed manually in the

software from the orthogonal view of both cells and nuclei. Knowing these parameters, the flatness index (FI) was calculated as the ratio between major axis and thickness.

The nuclear-cytoplasmic YAP ratio was quantified using the strategy developed by *Nardone* et al. [18] using this equation:

$$\frac{\sum_{nuc}^{l} pixels \Big/ A_{nuc}}{\sum_{cyto}^{l} pixels \Big/ A_{cyto}}$$

where $\sum_{nuc}^{l} pixels$ and $\sum_{cyto}^{l} pixels$ represent the sum of the intensity values for the pixels of YAP proteins in the nuclear and cytoplasmic region, respectively, whereas A_{nuc} and A_{cyto} are the area of the corresponding regions.

To visualize the actin cap on the nucleus, we processed the z-stack images acquired for the actin (phalloidin) and the nucleus (DAPI) with Fiji. The bottom half of the actin z-stack was cancelled to remove basal actin fibres from the analysis. The remaining top half was z-projected and sharpened. Similarly, the nucleus z-stack was z-projected, and the projected image was duplicated and binarized using "Li" threshold. The binary image was used to construct a mask to restrict the actin image to the nuclear region only.

2.1.5. Statistical analysis

Data are reported as mean ± standard error of the mean (SEM). Experiments have been performed in triplicate. Statistical comparisons were performed with ANOVA followed by Tukey's test for multiple comparisons on 20 cells at 24 h and at least 10 cells at reference configuration and 48 h. P values of <0.01 or <0.05 denote statistically significant differences.

2.2. Simulative Part

2.2.1. Finite element simulations

Finite element (FE) simulations were performed using ABAQUS 2022 (Dassault Systémes Simulia Corp.). In the 3D FE model, the cell is assumed as a structure composed of nucleus, cytoplasm, and actin cap. Cell and nucleus are modelled as compressible isotropic Neo-Hookean hyperelastic materials with different mechanical properties. The materials were both considered compressible because, in the large displacement fields, volume variations were previously recorded [22,23]. The Young's modulus, *E*, for nucleus and cytoplasm is 4000 and 500 Pa [22, 24–26], respectively, and the Poisson's ratio $\upsilon = 0.35$ [22,27]. A perfect connection at the nucleus-cytoplasm interface was assumed [22,28]. The micropatterned substrate is made of glass, which is simulated as a linear incompressible elastic material with Young's modulus E of 50 GPa. In the initial configuration, cytoplasm and nucleus are assumed to behave as two perfectly concentric 3D spheres having a diameter of 12 μm and 7.2 μm, respectively, quantified from experimental images into undeformed configuration (cells seeded on glass, fixed and visualized after 1 h that is considered the incipient phase of the spreading process). The external part of the cell is perfectly in contact with glass substrate in order to avoid the interpenetration of the cell into pattern during the spreading. Cytoplasm, nucleus and substrate are modelled with the same mesh element: solid continuum element of the first order with 8 nodes and hybrid formulation (C3D8H). The element size of cytoplasm and nucleus is 500 nm and the total number of solid elements for all model was 8016 with 8716 nodes. For each experimental case, a 3D finite element simulation was carried out in order to reproduce the stretching of the whole-cell on the substrate. To this scope, a proper experiment-derived displacement field was applied on the cytoplasmic surface in cylindrical coordinates (see Supplementary Material – The 3D Finite Element Model Approach).

Moreover, the action of the actin cap on the nuclear surface was simulated by applying distributed nodal forces on a specific area of interest corresponding to the observed extent. This force is quantified knowing the pressure exerted by actin cap on the nucleus, equal to 816 Pa [23], and the surface of interest where it is applied (quantified from experiments) (see Supplementary Material – The 3D Finite Element Model Approach, Fig. S2 S-V). As a result, the distributed force corresponds to 27.91 nN for R1 and R2 micropatterns, 20.09 nN for C2 adhesive islands and 0 Nn for C1.

From the 3D FE macro-model simulation results, all the displacements and stresses developed on the 3D solid nuclear outer surface were retrieved and used as kinematic boundary conditions in the formulation of the 2D meso-models. In particular, specific representative surface (RS) regions of the nuclear envelope were considered to perform meso-scale simulations: top surface and side part. Each one of the NE RSs had an area of 4 μm^2 containing a number of 20 uniformly distributed pores (5 NPC/μm^2) [15]. The NE RS is designed as a deformable 3D shell with a thickness of 120 nm [10] and includes pores as circular concentric structures having external and internal diameter of 120 nm and 60 nm, respectively and a thickness of 60 nm [29–31]. The NE RS is assumed as an isotropic hyper-elastic incompressible material having a shear modulus (μ) equal to 10^4 Pa [23]; the same constitutive behaviour is considered for the NPCs 2D structure except for the Young's Modulus assumed as 1 MPa [32]. Indeed, from literature evidences [32], it results that the NPCs are more rigid with respect to the NE, so in our 2D FE meso-model, the nuclear rings, which simulate the NPCs, have a higher stiffness compared to the nuclear envelope. The mesh element used for 2D models is 4-node curved thin shell of the first order with the reduced integration (S4R) and the total number of element results equal to 8545 with an element size of 25 nm and 8802 nodes. Depending on the 3D macro-model results considered, a proper specific displacement field in cartesian coordinate was applied to the edges of the shell RS, including the periodic constrains to consider the remaining parts of the surfaces.

3. Results

3.1. Cellular confinement affects cytoskeleton assembly and cellular shape

Surface micropatterning proved to be effective in modulating cytoskeleton architecture and, consequently, global cell shape and structure since it provides large adhesive areas permissive for the formation of cell adhesions alternated with not permissive ones [33].

We firstly observed that the organization of actin cytoskeleton and the formation of stress fibres at 24 h strongly depended on the shape of the adhesive islands when adipose stem cells were cultured on 1300 μm^2 ones. In fact, a disorganized meshwork of thin actin filaments with several filopodial protrusions were detectable when ASCs were cultured on small circular patterned surfaces (C1), with cortical actin retracing the contour of the coated adhesive island (Fig. 1A, S3A). On the contrary, actin bundles running along the main sides of small rectangle adhesive islands (R1) were detected (Fig. 1B). In fact, we observed that the cytoskeleton of ASCs cultured on R1 patterned substrates was prevalently constituted by packed actin stress fibres oriented along the major axis of the elongated ASCs (Fig. S3B). However, when ASCs were cultured on 5000 μm^2 adhesive areas, even if thick stress fibers were detectable on both patterned surfaces, different actin cytoskeleton assemblies were observed (Fig. 1C and D). On large circular adhesive areas patterned surfaces (C2), radial arrangements of thick actin bundles – resembling dorsal stress fibres – and circumferential actin fibres possessing the typical concentric organization of transverse arcs over the whole cellular body (Fig. S3C) were observed. On the contrary, thick actin fibres crossing whole cellular body were obtained when ASCs were cultured on large rectangular adhesive areas (R2) (Fig. S3D) suggesting that the shape of the adhesive islands played an important role in dictating cytoskeletal actin fibres maturation and organization.

Then, we evaluated cell morphometric parameters, i.e., cell area, thickness, and flatness index (FI) for all the experimental conditions. Starting from the cell area (Fig. 1E), each ASC spreads throughout the

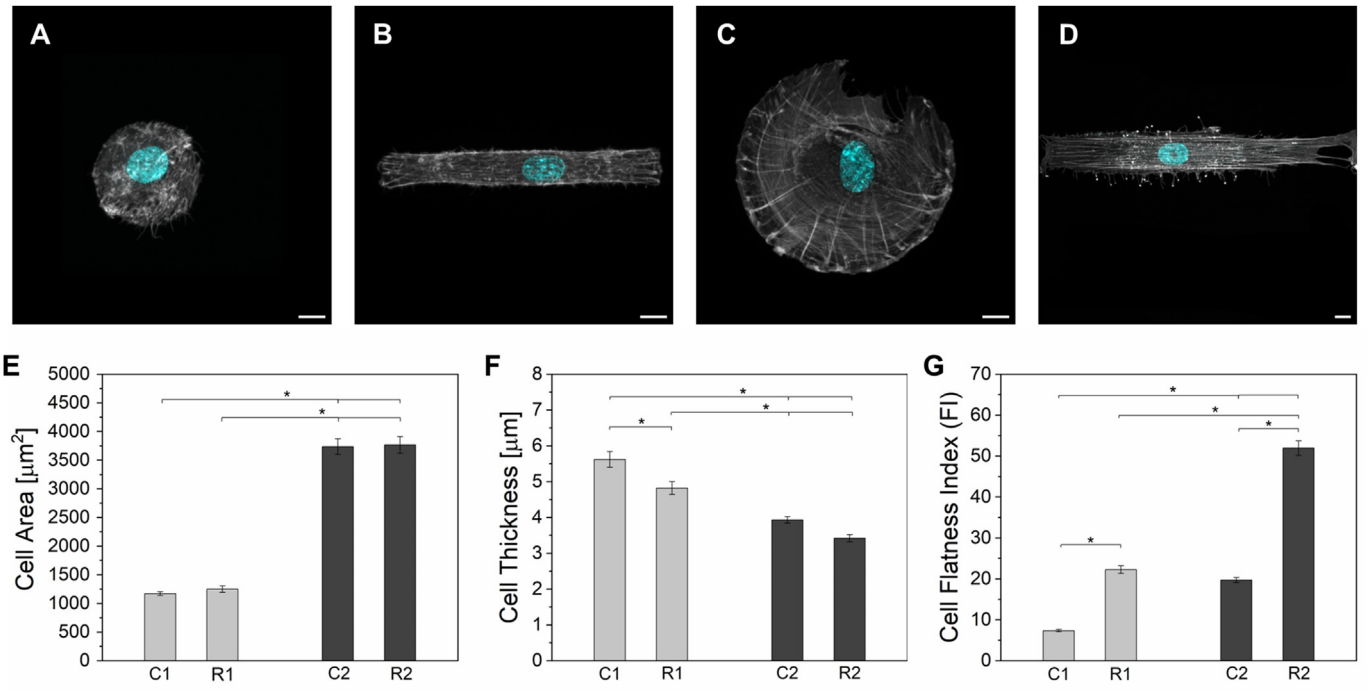

Fig. 1. Actin cytoskeleton (grey) and nuclei (cyan) confocal images of single ASCs cultured on C1 (**A**), R1 (**B**), C2 (**C**) and R2 (**D**) patterned surfaces for 24 h. Scale bar is 10 μm. Histogram of cell area (**E**), cell thickness (**F**) and cell flatness index (**G**) of single ASCs cultured on patterned surfaces. The results are expressed as data ±s.e.m. considering 20 cells from three independent experiments for each configuration. *$p < 0.01$ statistical differences (where not indicated, the statistical differences are not significant).

entire R1 pattern (1250 ± 250 μm^2) and there was an almost complete spreading also on C1 (1171 ± 139 μm^2) after 24 h of culture. Conversely, we observed that ASCs cultured on larger adhesive patterned surfaces reached their maximum spreading configuration after 24 h too, but they were not able to cover the whole adhesive surface area since ASCs cultured on C2 and R2 covered an average area of 3734 ± 606 μm^2 and 3765 ± 692 μm^2 respectively, which correspond to ~74% and ~75% of the entire pattern.

In addition, we observed that cell thickness decreased with the increasing of ASC spreading (Fig. 1F). In fact, for patterns C1 and R1, cell thickness resulted equal to 5.62 ± 0.96 μm and 4.82 ± 0.80 μm, respectively, whereas for C2 and R2 was 3.93 ± 0.39 μm and 3.42 ± 0.46 μm. These results indicated that the smaller is the thickness of ASCs spread on different patterns, the higher is the compression at which the cells are subjected along the vertical direction.

We also quantified cell flatness index (FI), obtained as the ratio between the major axis and the thickness of the ASC after spreading (Fig. 1G). A smaller FI value was found for ASCs cultured on C1 patterned surfaces (7.33 ± 1.33) with respect to those calculated for ASCs cultured on R1 (22.26 ± 4.10) and C2 patterned surfaces (19.71 ± 2.62). However, the highest cell flatness index was observed for ASCs cultivated on R2 patterned surfaces (51.93 ± 8.41), where the cells displayed the most elongated shape.

To verify whether the morphological features of cells were stable at longer times, we performed the same image analysis at 48 h for all patterned configurations. Cell Area, (Fig. S4A), cell thickness (Fig. S4B) and cell flatness index (FI) (Fig. S4C) measured at 48 h were not significantly different from the data measured at 24 h.

3.2. Cellular shape and spreading differently affected actin cap assembly and nucleus morphology

The perinuclear actin cap was recently characterized as a supramolecular structure constituted by thick, parallel, and highly contractile acto-myosin filaments, that are specifically anchored to the apical surface of the nucleus [5]. Here, we observed that cellular shape impacted the formation of the ASC actin cap. In fact, when ASCs were cultivated on C1 patterned surfaces, no actin cap was detected after 24 h of culture but only small patches or discontinuous whiskers, whereas the actin cap formation was observed when ASCs were cultured on R1 substrates (Fig. 2A and B, Fig. S5). Conversely, ASCs formed actin cap irrespective of their shape (circular or rectangular) when they were cultured on large adhesive islands patterned surfaces (C2 and R2) (Fig. 2C, D, Fig. S5). When formed, the actin cap was evident in the form of a parallel array of fibres with a clear and uniform orientation. Conversely, on the C1 case, we observed a broad distribution of orientations of the small and discontinuous whiskers (Fig. S5). Moreover, we also quantified the actin fibre thickness in the different configurations having 0.28 ± 0.05 μm (R1), 0.29 ± 0.06 μm (C2) and 0.29 ± 0.05 μm (R2) (Fig. S5).

Since actin cap is directly connected to the nuclear lamina and nuclear envelope through LINC complexes [34], we expected that the morphology and the shape of the nucleus could be differently affected by the presence/absence of the cell actin cap. To this aim, morphological features of nuclei (area, thickness, aspect ratio, and flatness index) were calculated for all tested conditions.

The projected nucleus area depends on the area of the adhesive islet but does not depend on its shape (Fig. 3A). In fact, C1 and R1 have a similar nucleus area (157 ± 24, 143 ± 23 μm^2) and the same occurs for C2 and R2 (205 ± 42, 205 ± 32 μm^2). As shown in Fig. 3B, the nucleus AR, assessed as the ratio between the major and minor axis of the nucleus after spreading, was similar in ASCs cultivated in the various configurations (C1 = 1.32 ± 0.13, C2 = 1.27 ± 0.18 and R2 = 1.41 ± 0.14) with the only exception of nuclei of ASCs cultured on R1 patterned surfaces (1.62 ± 0.23), on which they displayed more oblate nuclei with respect to other experimental conditions. Moreover, nuclei were thicker when cells spread on small patterns (C1 = 4.76 ± 0.92 μm, R1 = 4.11 ± 0.66 μm) with respect to those on larger ones (C2 = 3.84 ± 0.78 μm, R2 = 2.98 ± 0.49 μm) (Fig. 3C).

Then, the FI of the nucleus, here calculated as the ratio between the major axis of the nucleus and its own thickness, was small for C1 (3.57 ±

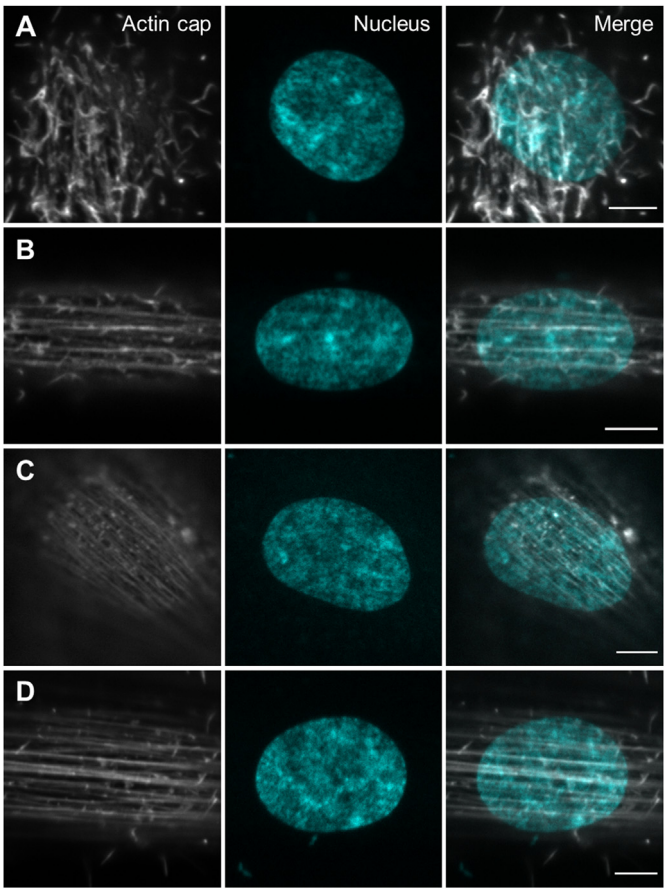

Fig. 2. Representative confocal images of cell actin cap (grey) and nuclei (cyan) of single ASCs cultured for 24 h on C1 (**A**), R1 (**B**), C2 (**C**) and R2 (**D**) patterned surfaces. Scale bar is 5 μm.

0.89) and large for R2 (6.58 ± 1.19) (Fig. 3D). This parameter assessed the nuclear stretching, which was minimum on the small circular adhesive islands patterned substrates and maximum on the large rectangular one. Intermediate results were obtained for R1 (4.26 ± 0.82) and C2 (4.92 ± 1.53). Altogether, these data suggest that cellular elongation on large adhesive patterned surfaces promoted nuclear stretching through a specific assembly of actin cap cytoskeleton, mainly constituted by an aligned array of thick actin fibres able to exert high compressive forces on the top of nucleus surface, eventually modifying its morphology.

Also, for the nucleus, a comparison of morphometric results was made at 24 h and 48 h to assess the stability of nuclear shape at a longer timepoint. Nucleus area (Fig. S4D), thickness (Fig. S4E), aspect ratio (Fig. S4F) and flatness index (Fig. S4G) measured at 48 h were not significantly different from the data measured at 24 h.

3.3. Nucleus morphology modulates YAP nuclear/cytoplasm trafficking

YAP proteins are transcriptional regulators involved in cell differentiation, proliferation, and survival; therefore, they are classified as mechanotransducers [7,8,11,18–20,35]. To analyse how cell confinement and nuclear deformation influenced nuclear-cytoplasmic trafficking of YAP and what was the type of transport with which they move, the nuclear-cytoplasmic YAP ratio is herein quantified under different experimental conditions.

The nuc/cyt YAP ratio was quantified using the protocol developed by *Nardone* et al. [18] as the ratio between the fluorescence intensity of YAP in the nucleus and cytoplasm normalized with respect to its own area (Fig. 4A). The nuc/cyt YAP ratio approximates two when there is a uniform distribution of proteins between cytoplasm and nucleus [18], which is what we found in cells cultured for 24 h on C1 (1.94 ± 0.71) and R1 (2.00 ± 0.71) patterned surfaces (Fig. 4B and C). Conversely, YAP presented a preferential nuclear localization when cells increased their spreading area [18]. In fact, cells cultured on patterned surfaces of large adhesive areas (C2 and R2) showed an increased accumulation of YAP into the nucleus with respect to the cytoplasm (C2 = 6.39 ± 1.95 and R2 = 5.35 ± 1.67) (Fig. 4D and E). As a result, the nuc/cyt YAP ratio was directly correlated with the spreading area of the ASCs (C1–C2, R1-R2) but was not related to the shape of the area itself. In fact, there were not statistically differences between C1-R1 and C2-R2.

To verify whether time-dependent redistribution of YAP occurred on each pattern shape, we measured nuc/cyt YAP ratio at 48 h and compared this to the 24 h case (Fig. S4H). The ratio measured at 48 h for C1, C2, and R1 micropatterns was similar to the corresponding ratio at 24 h. Only for R2 adhesive island, the nuc/cyt YAP ratio at 24 h was found to be higher with respect to that measured at 48 h (Fig. S4H).

3.4. Numerical approach to macroscopically simulate the cellular and nuclear spreading

To simulate cell spreading on the differently shaped patterns, a full 3D FE macro-model, including cytoplasm, nucleus, and actin cap, was formulated for each configuration herein investigated. The cell spreading was reproduced within the finite deformation hypothesis and through the application of a specific experimental-derived displacement field on the cell outer surface (see Simulative Part in Materials and Method). Specifically, the kinematic equations of the displacement fields were formulated to reproduce in the model the same cell morphology quantified into the experiments after 24 h of culturing. Then, the 3D simulation results were utilized to replicate the NE confinement/deformation conditions at a smaller scale of observation, i.e., creating a periodic-meso 2D FE model of the NE which includes the openings of the NPCs and corresponding mechanical characteristics. The openings representing the NPCs were surrounded by a stiffer circular region to reproduce cytoplasmatic rings [32] lying on the NE. The representative periodic-meso NE surfaces belong to both top and side part of the NE, being to the most stretched areas of the nucleus after spreading (Fig. 5). In detail, the transmission of the stress state to the nucleus due to cell confinement generates a specific displacement field on the NE surface (from the undeformed configuration); thus, this field was used as kinematic boundary condition into the formulation of the 2D meso-model. In this way, the response of the NPCs to the different cell stretching conditions was numerically assessed.

In Fig. 6A, Videos S1–S4 the different displacement fields obtained on the cell surface from 3D FE simulations are shown for all pattern situations. To validate the numerical approach, the cell area, and the cell thickness (Fig. 6B) in experiments and simulations were compared. For both cell area and cell thickness after spreading, all the quantities evaluated with the FE model were in good agreement with the experimental results.

Then the von Mises stress developed on the cellular surface in the different configurations have been also analysed. As shown in Fig. S6, a similar von Mises stress distribution was quantified between rectangular pattern R1 and circular islet C2 even if the cell spreading area in the first case was smaller with respect to the second one. Furthermore, for patterns R1 and R2 having the same shape but different spreading area a similar von Mises stress distribution has been obtained. On the contrary, for C1–C2, the larger is the cell spreading the higher is the stress developed on the cellular surface.

Focusing on the effects of cell shape and spreading on nucleus deformation, the nucleus displacement field developed on its surface in the different cases is reported in Fig. 7A, Videos S5–S8. The greater the cell spreading, the larger the nuclear stretching. A comparison of the nuclear area (Fig. 7B) between experiments and FE 3D models showed an under-estimation of nuclear stretching into simulations with respect to experiments for all configurations. On the contrary, a good agreement

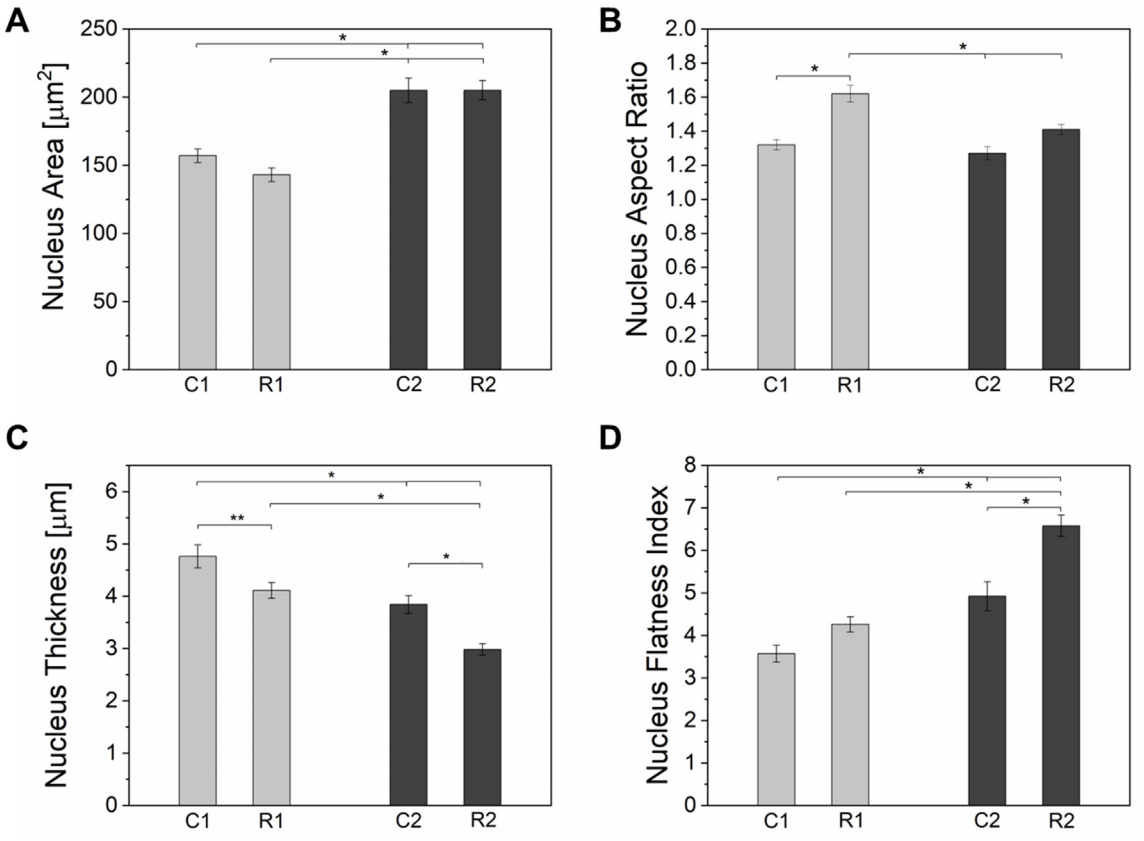

Fig. 3. Histograms of cell nucleus area (**A**), nucleus aspect ratio (**B**), nucleus thickness (**C**) and nucleus flatness Index (**D**) of single ASCs cells cultured on patterned surfaces at 24 h. The results are expressed as data ±s.e.m. considering 20 cells from three independent experiments for each case. *$p < 0.01$; **$p < 0.05$ statistical differences (where not indicated, the statistical differences are not significant).

was observed for nuclear thicknesses comparing experimental results with the numerical ones.

Supplementary video related to this article can be found at https://doi.org/10.1016/j.mtbio.2022.100335

Then the von Mises stress developed on the nuclear surface gave another important information about the role of shape pattern and perinuclear actin cap on the nuclear stretching. In fact, as shown in Fig. S7, a more intense stress field was developed in the rectangular pattern R1 than C2 even if the cell spreading in the first case was smaller with respect to the second one. Furthermore, for patterns having the same shape but different spreading area (C1–C2, R1-R2), the larger is the cell deformation the higher is the stress developed on the nuclear surface and the maximum is obtained on the R2 islet.

3.5. *Periodic-meso 2D FE model to simulate the NPCs response to the different nuclear spreading configurations*

The displacement fields developed on the nuclear surface from the initial to the stretched configuration of the full 3D FE model (Fig. 7) were used as kinematic boundary conditions and applied to representative surfaces of the NE containing the NPCs. The goal was to analyse the response of NPCs to the different simulated mechanical cues. The regions of the NE chosen as representative surface elements are the top surface and the lateral one on the equatorial plane, since they are representative of different displacement and stress fields (Figs. 5 and 7A, S7). Two different lateral regions of nuclei of cells on the rectangular patterns were considered: one located by the pointed end orthogonal to the x axis (lateral part 1), the other one located by the blunt side orthogonal to the z axis (lateral part 2) - (see Fig. 5 for reference). This choice was motivated by the fact that in these two regions the nucleus experiences markedly different displacement fields (Fig. 7A).

Conversely, only one lateral region of nuclei of cells on circular patterns was considered, owing to the isotropic spreading and consequent homogeneity of the displacement fields along the equatorial line. To analyse how cellular and nuclear spreading influence the NPCs response, the shape, and the area of the internal ring of these structures were assessed at the end of simulation, since this is the region of NPCs through which TFs can pass from the cytoplasm to the nucleus and vice-versa. The total deformed NPC area (i.e., corresponding to the summation of the areas of all the deformed NPC openings belonging to the representative 2D periodic-meso NE surface) was assessed in different nuclear spreading situations and it was evaluated with respect to the Nuc/Cyt YAP ratio observed in the experiments (Fig. 8A). For all the configurations, there was an increase of NPCs area with respect to undeformed configuration, in which the total area of the NPC openings was equal to 2827 nm^2 per 4 μm^2 of the representative NE surface (Fig. 8A, black straight line); however, only for the larger patterns (i.e., C2 and R2) an accumulation of YAP inside the nucleus was observed and possibly related to NPC area changes. On the top surface region (Fig. 8A – red squares), the total simulated NPCs area of the representative NE surface was smaller for C1 (3385 ± 63 nm^2) and R1 (3450 ± 71 nm^2) than C2 (3969 ± 76 nm^2) and R2 (4400 ± 74 nm^2). As the representative surfaces contain the same pore density (5 NPC/μm^2) an increase in the total area corresponds to an increase of the average pore area. In fact, NPC area passed from +20 to 22% to +41–56% and this can be directly correlated with the enhanced nuclear spreading. Hence, the larger is the nuclear stretching the higher is the openings developed on the NPCs belonging to the top part of the NE (Fig. 8C). To study the shape assumed by the pores at the end of nuclear stretching step, the NPC aspect ratio (AR_{NPC}) was quantified (Fig. 8B). This was measured as the ratio between the major and the minor axis of the deformed NPCs (whereas it is equal to 1 in the case on undeformed NPCs). On the top surface (Fig. 8B – red squares), for circular patterns

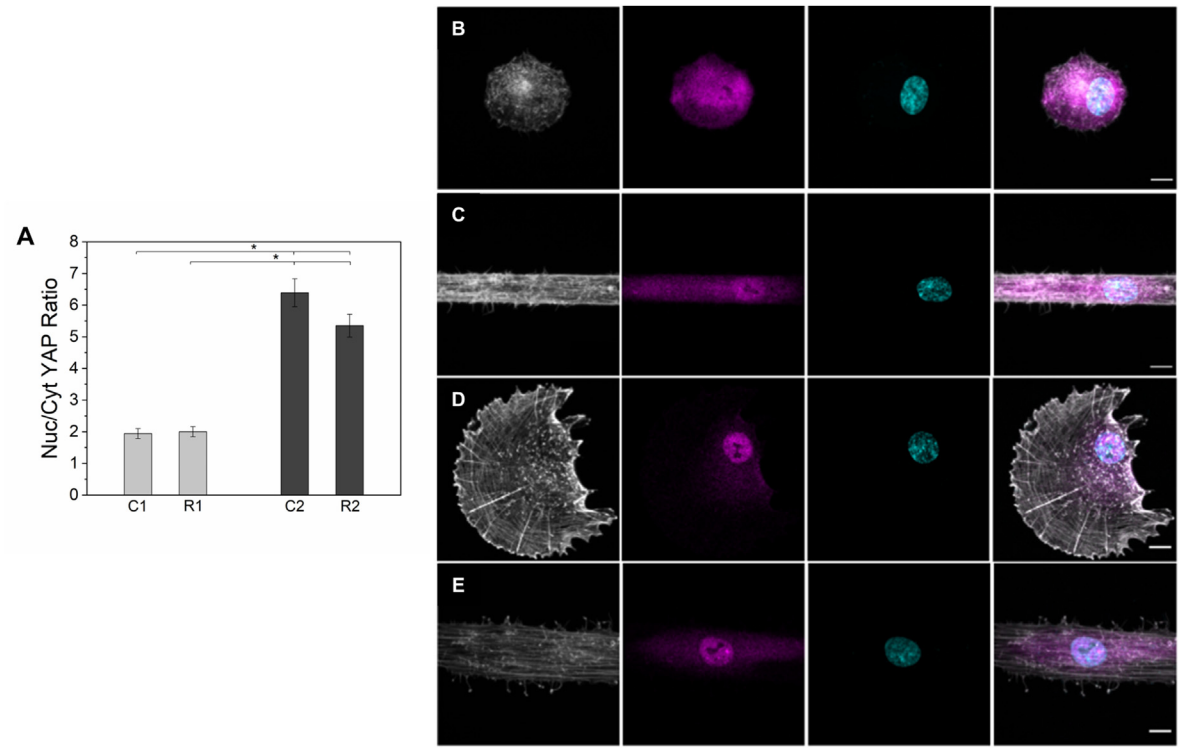

Fig. 4. **A** Histograms of Nuc/Cyt Yap ratio for all experimental condition tested. The results are expressed as data ±s.e.m. considering 20 cells from three independent experiments for each case. *$p < 0.01$ statistical differences (where not indicated, the statistical differences are not significant). (**B-E**) Actin (grey), Yap (magenta) and nucleus (cyan) representative confocal images of single ASCs cultured onto fibronectin-coated micropatterned surfaces (B, C1. C, R1. D, C2. E, R2). The scale bar for all images is 10 μm.

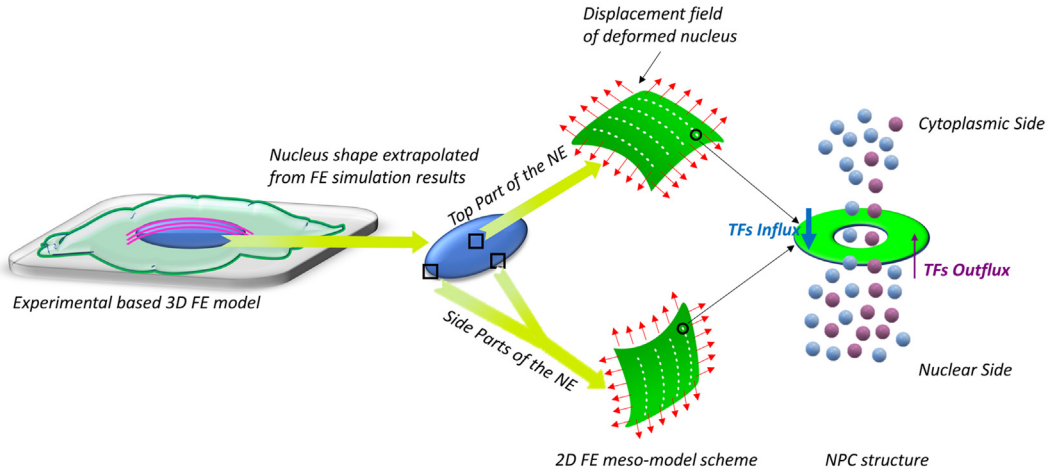

Fig. 5. Schematic representation from experimental based 3D FE macro-model to the 2D FE meso-model scheme with a zoom on NPC structure.

(C1, $AR_{NPC} = 1.01 \pm 0.02$ and C2, $AR_{NPC} = 1.02 \pm 0.02$) the AR_{NPC} is close to 1, which means that there was not a preferential direction of the opening shape but only an increase of area; this result also reflected the symmetry of the nuclear spreading. On the contrary, the aspect ratio of the NPCs increased for rectangular patterns (R1, $AR_{NPC} = 1.48 \pm 0.03$ and R2, $AR_{NPC} = 1.38 \pm 0.04$) due to the preferential direction of cellular stretching propagated on NPCs behaviour. For the top surface regions, the 2D meso-models showed an area of NPCs higher for large patterns with respect to the smaller ones, which is perfectly correlated with the experimental profile of the nuc/cyt YAP ratio.

A different result was observed for the side regions of the deformed nuclei (Fig. 8A – green/yellow circles and rhombuses) where, for all configurations, the NPCs area was close to 3000 nm^2 regardless of nuclear stretching.

Analysing the NPC ARs (Fig. 8B – green/yellow circles and rhombuses) and the displacement field developed on the NPCs (Fig. 8D, E), a heterogeneity of results was obtained. Particularly, a preferential distortion was observed along the z axis for C1 ($AR_{NPC} = 1.30 \pm 0.03$), C2 ($AR_{NPC} = 1.34 \pm 0.03$) and R2 ($AR_{NPC} = 1.31 \pm 0.06$) in the lateral part 1 and along the x axis for R1 ($AR_{NPC} = 1.96 \pm 0.04$) and R2 ($AR_{NPC} = 2.43 \pm 0.08$) in the lateral part 2. A preferential stretching direction for R1 ($AR_{NPC} = 1.08 \pm 0.04$) pattern in the lateral region 1 was not observed. Since the lateral part 1 is that located by the pointed end orthogonal to the x axis, whereas the lateral part 2 that by the blunt side orthogonal to the z axis, the NPC response is a combination of displacement fields due to nuclear elongation along the x-z axes and compression along the y one.

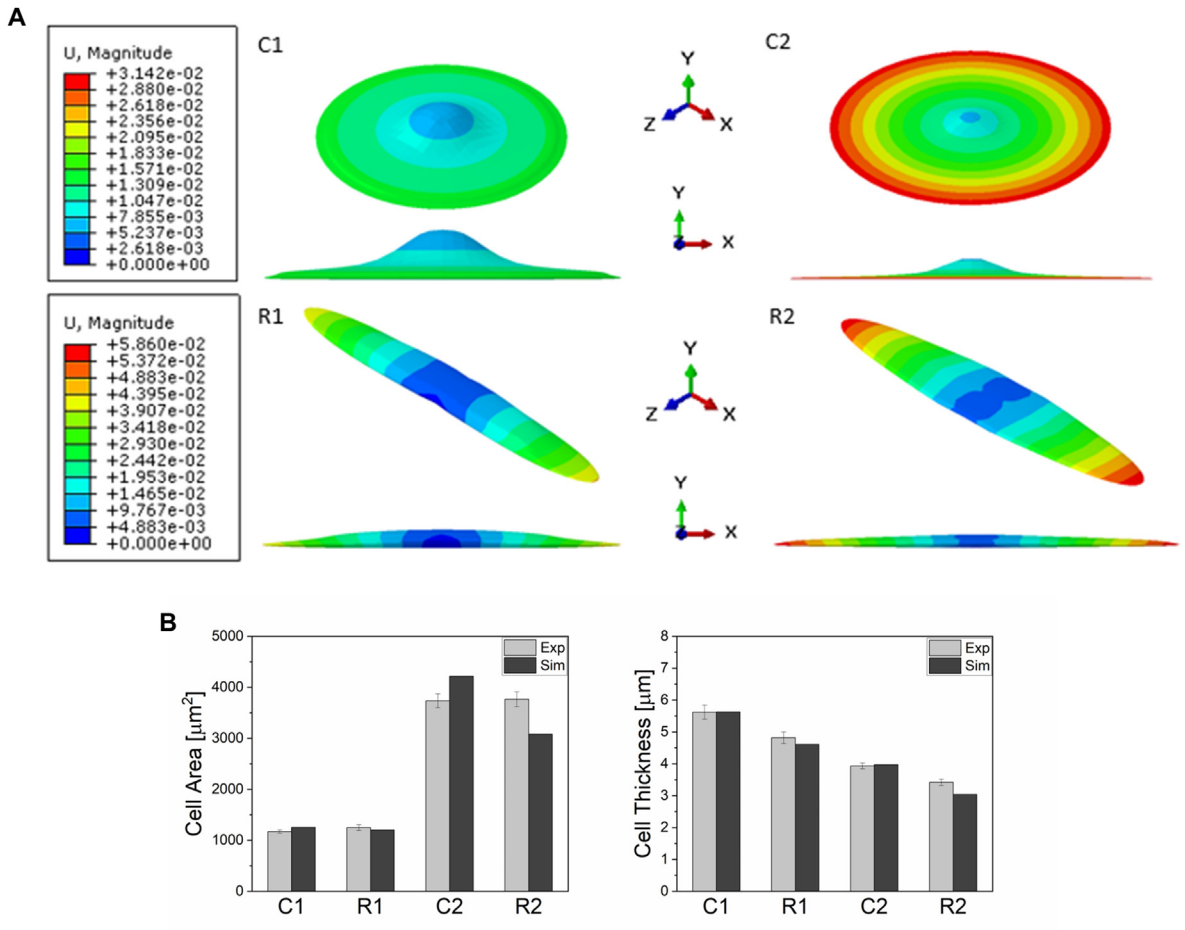

Fig. 6. (**A**) Displacement field for all patterns developed on cell surface during the cell spreading (displacement in contour plot expressed in mm); (**B**) Experimental and simulation results in terms of cell area and cell thickness for the validation of macro-models. The experimental results are expressed as data ±s.e.m. considering 20 cells from three independent experiments for each case.

If a correlation between NPCs stretching and YAP shuttling is demonstrated from the periodic-meso 2D FE models on the top part of nuclei, the same was not observed on the lateral part where the combination of displacement fields changed their shape but not their area irrespective of the considered pattern.

4. Discussion

The cytoplasmic/nucleus shuttling of TFs is an important process that regulates a variety of cellular behaviour with high efficiency [7,8,18,19]. Several models have been proposed to describe the dynamics of TFs translocation. For instance, the binding of Myocardin-related transcription factor A with monomeric G-actin prevents the translocation of the TF into the nucleus. Sequestration of G-actin caused by actin polymerization and cytoskeleton assembling frees the TF making it available for nuclear transport [36]. YAP belongs to those TFs whose shuttling dynamics is sensitive to the cell's cytoskeletal structure [37,38]. It is a transcriptional coactivator downstream of the Hippo pathway that regulates many cellular functions, such as proliferation, migration, differentiation, and apoptosis [7,8,18,19]. Many findings have demonstrated that YAP is also a protein that respond to extracellular environment signals as its rigidity and geometry, cell density and polarity and the intracellular status of the actin cytoskeleton, altogether determining a peculiar nucleus/cytoplasm localization [39]. For these reasons, there is a growing interest in understanding how exogenous mechanical signals or endogenously generated forces affect YAP localization and hence its activity. However, irrespective of the specific transport mechanism, nuclear translocation ultimately requires the crossing of the nuclear membrane through NPCs. Therefore, it is likely that altered morphologies of NPCs can affect TF translocation dynamics. Therefore, changes in NPCs size would have a major role on the dynamics of molecules of this type. However, it is unclear how the intracellular stress state alters the morphology of NPCs and how this affects the TFs crossing through the NE. A recent work by Elosegui-Artola et al. [7] reported that stretched nuclear pores are observed in cells cultivated on stiff substrates, a condition that improved cell contractility and nucleus flattening. Such a pore configuration promotes YAP nuclear influx as opposed to what observed in cells cultivated on compliant substrates, for which case YAP nuclear influx and outflux are balanced. Achieving an accurate and clear representation of the distribution of NPC shapes in various experimental/boundary conditions is technically cumbersome, as it is difficult to acquire representative regions of interest of the nuclear membrane with electron microscopic techniques. However, either meso-scale mechanical or numerical models, can be useful to partially overcame this technical limitation, providing a valuable insight on how nanoscale nuclear pores change their morphological features according to deformations occurring at the whole nucleus level.

To this aim, we considered the changes of YAP induced by nuclear stretching by determining the corresponding accumulation in either the cytoplasm or the nucleus of ASCs cultivated on micropatterned surfaces possessing different shapes and adhesive culturing areas. The experimental results showed a variation of cellular spreading and nuclear shape induced by different cytoskeleton assemblies associated to the shape and dimension of the adhesive island of the pattern adopted. Cell and nucleus morphological features did not change from 24 to 48 h, suggesting that the mechanical inputs provided by the micropatterned substrates were

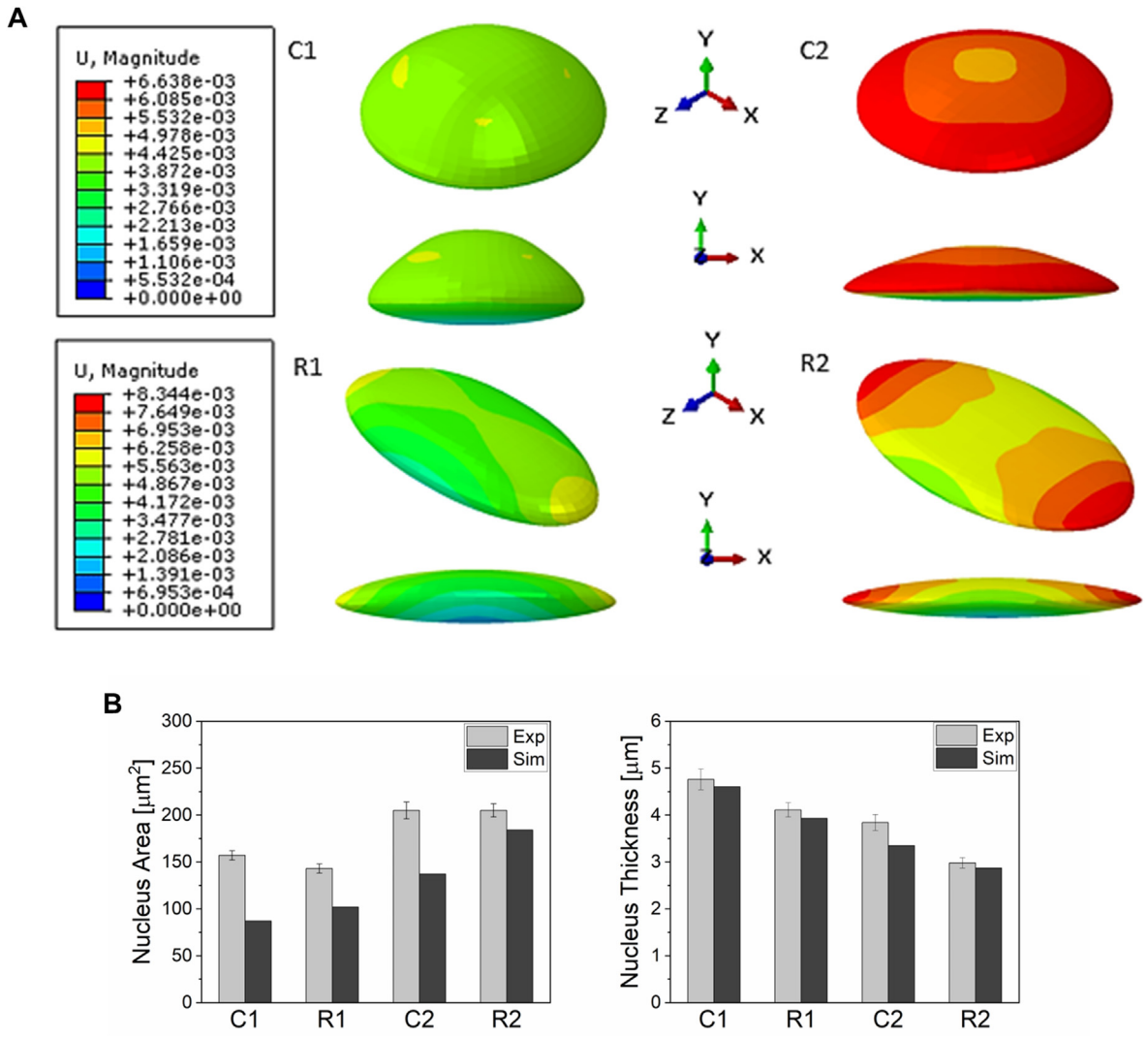

Fig. 7. (**A**) Displacement field for all patterns developed on nuclear surface during the cell spreading (displacement in contour plot expressed in mm); (**B**) Experimental and simulation results in terms of nucleus area and nucleus thickness. The experimental results are expressed as data ±s.e.m. considering 20 cells from three independent experiment for each case.

temporally stable and hence our model can be applied within this timeframe. It must be pointed out that at 48 h cell proliferation is observed on the substrates in which case islets are colonized by multiple cells, displaying diverse cell and nuclear morphology. Beyond 48 h the proliferation is so extensive that virtually no isolated cells are observed. In this scenario, the micropatterns lose their function of homogenizing the mechanical inputs and it is difficult to define the shape of the cell final configurations to be used as targets in the computational model. Within the boundaries of our experimental setup, the different deformed shapes and confinement conditions characterizing the nucleus generated a different nuc/cyt YAP ratio. Particularly, in the cases of substrates with the same micropattern shape but different dimensions, as C1 and C2 or R1 and R2, an increase in terms of pattern size generated a raise of cell and nuclear spreading. This turned out into an increase of the nuc/cyt YAP ratio (Fig. 4, Fig. S4H), possibly generated by a YAP in-flux which dominated on the out-flux, in agreement with Nardone et al. [18] and Elosegui-Artola et al. [7].

For micropatterns with the same spreading area but different micropattern shape, i.e., C1 and R1, C2 and R2, there is not a statistically significant nuc/cyt YAP ratio variation, even if it has been recently demonstrated that cellular elongation triggers YAP nuclear export through nuclear compressive forces exerted by the actomyosin network [8].

Moreover, comparing the nuc/cyt YAP ratio for C2 and R2 micropatterns at 24 h and 48 h, we found a slight decrease in the nuc/cyt YAP ratio at 48 h, a decrease that is statistically significant only for the R2 case, both of which – however – remain significantly higher with respect to the C1 and R1 cases (Fig. S4H). Although specific analyses are needed to characterize such a time variation of nuclear YAP in C2 and more specifically in R2, with our data we can speculate on the fact that at 48 h cells are prone to proliferate, for which case, YAP should be mostly nuclear [40]. We acquired isolated cells that, at this time point are likely to possess lower nuclear YAP quantities, a fact that inherently retard duplication. Therefore, at 48 h it is possible that, by restricting the analysis on the subpopulation of non-duplicated cells, we were actually sampling cells with lower nuclear YAP. This occurrence is likely to be less effective on small adhesive areas that are known to impair cell proliferation [41,42]. Also, it has been demonstrated that in epithelial cells during the G2/M phase, YAP is excluded from the nucleus [43]. Should this feature be common to ASC, as these cells approach the G2/M phase at longer culturing times, it is possible that we acquired cells richer in cytoplasmic YAP. Our model is based on a hyperelastic framework and does not consider time dependent phenomena arising, for instance from cell viscoelasticity or actin remodelling. Concerning cell and nucleus shape, within the time window we have explored, time dependent effects do not play a major role and hence our model can still describe nuclear

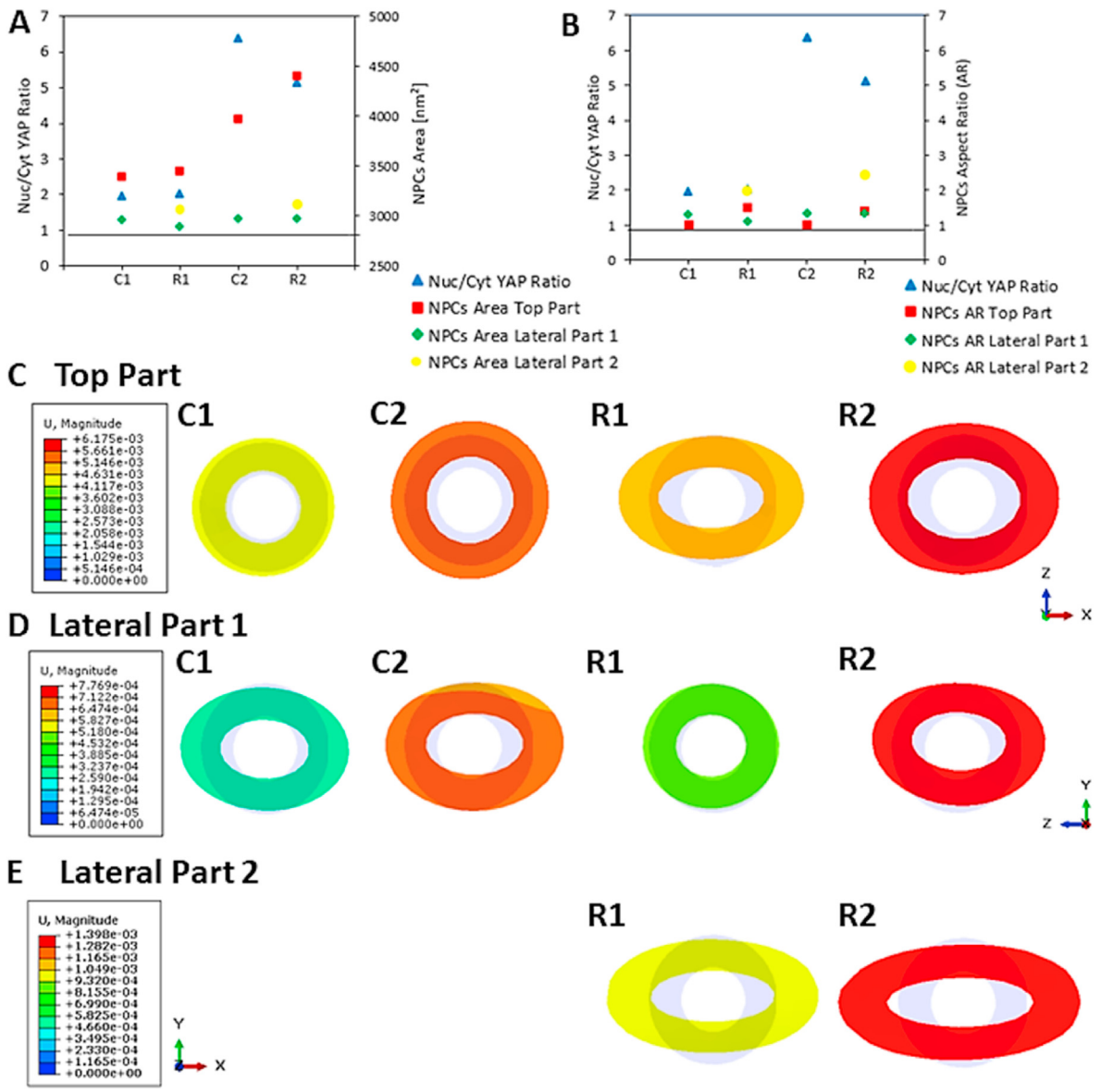

Fig. 8. **A**: Nuc/Cyt YAP ratio and NPCs Area [nm^2] for different pattern shapes and dimensions with respect to the top and the lateral parts of nuclei - black straight line shows the NPCs area into undeformed configuration; **B**: Nuc/Cyt YAP ratio and NPCs Aspect Ratio (AR) for different pattern shapes and dimensions with respect to the top and the lateral parts of nuclei - black straight line shows the NPCs AR into undeformed configuration; **C-E**: Overlapping of undeformed and deformed NPCs for different nuclear regions and pattern configurations - top part (**C**), lateral part 1 (**D**) and lateral part 2 (**E**) (displacement in contour plot expressed in mm).

mechanics. In particular, the periodic-meso 2D FE model we developed is able to replicate the NPCs response in different nuclear regions with respect to different nuclear stretching configurations. These 2D FE models were developed using as kinematic boundary conditions the displacement fields obtained by the 3D FE macro-models in correspondence of the nuclear surface. These models were able to replicate the cell spreading in the different confinement conditions with a good experimental correspondence in terms of cell area and cell thickness (Fig. 6). Such a good agreement with the experimental evidence allowed us to investigate in more depth NPC deformation arising from the confined cell spreading and the cytoskeleton forces.

From the simulation results and for all the cases investigated, we observed that the deformed NPCs exhibited different shapes and areas depending on the specific region of interest on the nuclear envelope. The top surface of the stretched NE is more prone to enlarge the openings of the NPCs whereas side regions are affected by vertical folding which modified the circular openings into oblong shapes (i.e., resulting in a different aspect ratio). Thus, focusing on the top part of the nucleus, ASCs cells cultured on C2 and R2 patterned surfaces, resulted into a larger internal area of the simulated NPCs with respect to the C1 and R1 cases (Fig. 8A – red squares). This result suggests that YAP might pass through sufficiently deformed NPCs with an influx rate (from the cytoplasm to the nucleus) larger than the outflux one, because of a specific level of applied nuclear stretch. In our experimental-numerical tests, such a nuclear stretch level is induced by the larger patterns rather than the smaller ones, as confirmed by the corresponding higher amount YAP accumulation inside the nucleus. Our results agree with those obtained by Garcia-Gonzàlez and colleagues [20], who showed a nuclear import of a small inert molecules (GFPs) through the NPCs depended on the strain state in the nuclear envelope which is faster in the spread configuration compared to the undeformed one. Moreover, the NPCs area in the top part changes from ~3500 nm^2 to ~4500 nm^2 (Fig. 8A). These areas have been quantified in the 2D FE meso-models starting from the diameter or major/minor axis of the circular and ellipsoidal pores, respectively. These dimensions are in the range 55–88 nm which are in good agreement with the NPCs dimensions found in Elosegui-Artola et al. [7], i.e.,

60–80 nm.

A different situation is observed for all the investigated patterns in terms of NPCs lying on the lateral regions of the nucleus, where the combination of displacements along x, y and z axes generated specific NPCs shapes which do not correlate with the YAP shuttling. In fact, their area in the deformed configurations is mostly the same of that computed into the undeformed state.

From the study of Das et al. [37] is evident that for low-density cells the integrity of the actin cytoskeleton becomes the dominant regulator of YAP nuclear localization. A well-structured cytoskeleton means an increase of the RhoA level which Kofler and colleagues [38] indicated as a central factor in the raise of YAP nuclear influx. From our experimental results, it is evident that a well-structured cytoskeleton is observed in cells spreading on the larger patterns (C2, R2) with respect to the smaller ones (C1, R1). The nuclear pore complexes deformation is correlated to the nuclear flattening generated by the mechanical loading of the cytoskeleton [7,38] and the pore deformation leads to the increase of their permeability. Since YAPs are proteins with a low mechanical stability [38], the YAP shuttling from the cytoplasm to the nucleus is likely to be facilitated by the combination of enhanced passive (i.e., stretched pores) and active transport mechanisms.

Our experimental and numerical results agree with the literature studies [7,18]. In fact, the YAP nuclear accumulation is observed for more stretched configurations (C2 and R2) which correspond to more deformed NPCs.

As far as the numerical approach is concerned, the novelty of the present study is the development of the periodic-meso 2D FE model to replicate the NPCs response as a function of nuclear stretching which, to the authors' knowledge, does not exist in the available literature. Our 3D macro-models share similarities with those developed by Nava et al. [22] and Milner et al. [28] even if they considered the cell as a structure composed only by the cytoplasm and the nucleus which behave as an incompressible material. Here, we introduced also the action developed by the actin cap on the nuclear response and the cell is simulated as a compressible structure. It is worth noting that, the propagation of cell spreading to the nuclear surface generated a stretching level of the nucleus which, on the numerical case, is smaller with respect to that showed by experimental results. This means that our macro-models slightly underestimated the nuclear deformation, even if all the dimensions are of the same order of magnitude (Fig. 7). This should be due to the constitutive relationship assumed for the nucleus. In fact, it has been considered as a compressible neo-Hookean hyper-elastic material (see Materials and Method) with a Young's modulus of 4000 Pa and even if this value agrees with other studies [24–26,44], the neo-Hookean law could be too simple for a complex material like the nucleus.

5. Conclusions

The YAP trafficking and NPCs responses are studied using an experimental and a numerical approach able to demonstrate the role played by the stretching in the modification of NPCs size and shape and how these conditions may be correlated to the YAP trafficking. A relationship between nuclear stretching, NPCs location, NPC aspect ratio and threshold levels of NPCs area changes might be inferred based on the observed variations in the YAP accumulation associated to the FE results. In principle, the mechanical gating predicted by our model might be applied to describe the trafficking through the nuclear envelope of other TFs or molecules having possibly size differing from that of YAP. Future studies need to experimentally observe the NPCs in the different stretching configurations and to improve the FE 3D macro and 2D meso models. Particularly, for the 3D FE macro-models, the osmotic pressure differences between the nucleus and the cytoplasm and the role of microtubules can be added, whereas for 2D meso-models the more complex structure of NPCs like nuclear basket could be considered.

CRediT author statement

Stefania Saporito: Conceptualization, Methodology, Software, Validation, Investigation, Writing - Original Draft, Writing - Review & Editing, Visualization. Carlo F. Natale: Methodology, Validation, Investigation, Writing - Original Draft, Writing - Review & Editing, Visualization, Funding Acquisition. Costantino Menna: Conceptualization, Methodology, Software, Supervision, Writing - Original Draft, Writing - Review & Editing. Paolo A. Netti: Resources, Supervision, Writing - Original Draft, Writing - Review & Editing, Maurizio Ventre: Conceptualization, Formal Analysis, Supervision Data Curation, Writing - Original Draft, Writing - Review & Editing.

Funding

This work was supported by a research grant from Compagnia di San Paolo – Università degli studi di Napoli Federico II (Star - L1 2017, DiSCEM project).

Data availability

The raw/processed data required to reproduce these findings will be made available upon requests to the authors.

Declaration of competing interest

The authors declare that they have no known competing financial interests or personal relationships that could have appeared to influence the work reported in this paper.

Appendix A. Supplementary data

Supplementary data to this article can be found online at https://doi.org/10.1016/j.mtbio.2022.100335.

References

[1] A. Garcia, J.F. Rodriguez Matas, M.T. Raimondi, T. M, Modelling of the mechano-chemical behaviour of the nuclear pore complex: current research and perspectives, Integr. Biol. (Camb) 8 (10) (2016) 1011–1021, https://doi.org/10.1039/c6ib00153j.

[2] B. Enyedi, P. Niethammer, Nuclear membrane stretch and its role in mechanotransduction, Nucleus 8 (2) (2017) 156–161, https://doi.org/10.1080/19491034.2016.1263411.

[3] K.N. Dahl, A.J. S Riberio, J. Lammerding, Nuclear shape, mechanics and mechanotransduction, circulation research, Circ. Res. 102 (11) (2008) 1307–1318, https://doi.org/10.1161/CIRCRESAHA.108.173989.

[4] D.H. Kim, et al., Actin cap associated focal adhesions and their distinct role in cellular mechanosensing, Sci. Rep. 2 (2012) 555, https://doi.org/10.1038/srep00555.

[5] D. H Kim, A.B. Chambliss, D. Wirtz, The multi-faceted role of the actin cap in cellular mechanosensation and mechanotransduction, Soft Matter 9 (23) (2013) 5516–5523, https://doi.org/10.1039/C3SM50798J.

[6] N. Wang, J. Tytell, D. Ingber, Mechanotransduction at a distance: mechanically coupling the extracellular matrix with the nucleus, Nat. Rev. Mol. Cell Biol. 10 (2009) 75–82, https://doi.org/10.1038/nrm2594.

[7] A. Elosegui-Artola, et al., Force triggers YAP nuclear entry by regulating transport across nuclear pores, Cell 171 (6) (2017) 1397–1410, https://doi.org/10.1016/j.cell.2017.10.008, e14.

[8] C. Bruyère, et al., Actomyosin contractility scales with myoblast elongation and enhances differentiation through YAP nuclear export, Sci. Rep. 9 (1) (2019), 15565, https://doi.org/10.1038/s41598-019-52129-1.

[9] M. Aragona, et al., A mechanical checkpoint controls multicellular growth through YAP/TAZ regulation by actin-processing factors, Cell 154 (5) (2013) 1047–1059, https://doi.org/10.1016/j.cell.2013.07.042.

[10] S.R. Wente, M.P. Rout, The nuclear pore complex and nuclear transport, Cold Spring Harbor Perspect. Biol. 2 (10) (2010), a000562, https://doi.org/10.1101/cshperspect.a000562.

[11] Matsuda, et al., On the nuclear pore complex and its emerging role in cellular mechanotransduction, APL Bioeng. 6 (2022), 011504, https://doi.org/10.1063/5.0080480.

[12] M.W. Hetzer. The nuclear envelope. Cold Spring Harbor Perspect. Biol.. 2(3): a000539. doi: 10.1101/cshperspect.a000539.

[13] H. B Schmidt, D. Görlich, Transport selectivity of nuclear pores, phase separation, and membraneless organelles, Trends Biochem. Sci. 41 (1) (2016) 46–61, https://doi.org/10.1016/j.tibs.2015.11.001.
[14] B.L. Timney, et al., Simple rules for passive diffusion through the nuclear pore complex, J. Cell Biol. 215 (1) (2016) 57–76, https://doi.org/10.1083/jcb.201601004.
[15] K. Ribbeck, D. Görlich, Kinetic analysis of translocation through nuclear pore complexes, EMBO J. 20 (6) (2001) 1320–1330, https://doi.org/10.1093/emboj/20.6.1320.
[16] D. Mohr, S. Frey, T. Fischer, T. Güttler, D. Görlich, Characterisation of the passive permeability barrier of nuclear pore complexes, EMBO J. 28 (17) (2009) 2541–2553, https://doi.org/10.1038/emboj.2009.200.
[17] Wolf, et al., Mechanotransduction: role of nuclear pore mechanics and nucleocytoplasmic transport, 2009, in: M. Mofrad, R. Kamm (Eds.), Cellular Mechanotransduction: Diverse Perspectives from Molecules to Tissues, Cambridge University Press, New York, 2009, pp. 415–435.
[18] G. Nardone, J. Oliver-De La Cruz, J. Vrbsky, J, et al., YAP regulates cell mechanics by controlling focal adhesion assembly, Nat. Commun. 8 (2017), 15321, https://doi.org/10.1038/ncomms15321.
[19] S. Dupont, Role of YAP/TAZ in cell-matrix adhesion-mediated signalling and mechanotransduction, Exp. Cell Res. 343 (1) (2016) 42–53, https://doi.org/10.1016/j.yexcr.2015.10.034.
[20] A.G. Gonzalez, et al., The effect of cell morphology on the permeability of the nuclear envelope to diffusive factors, Front. Physiol. 9 (2018) 925, https://doi.org/10.3389/fphys.2018.00925.
[21] A. Azioune, N. Carpi, Q. Tseng, M. Théry, M. Piel, Protein micropatterns: a direct printing protocol using deep UVs, Methods Cell Biol. 97 (2010) 133–146, https://doi.org/10.1016/S0091-679X(10)97008-8.
[22] M.M. Nava, R. Fedele, M.T. Raimondi, Computational prediction of strain-dependent diffusion of transcription factors through the cell nucleus, Biomech. Model. Mechanobiol. 15 (4) (2016) 983–993, https://doi.org/10.1007/s10237-015-0737-2.
[23] D.H. Kim, B. Li, F. Si, J.M. Phillip, D. Wirtz, S.X. Sun, Volume regulation and shape bifurcation in the cell nucleus, J. Cell Sci. 128 (18) (2016) 3375–3385, https://doi.org/10.1242/jcs.166330.
[24] G. Rosso, I. Liashkivich, V. Shanin, In situ investigation of interrelationships between morphology and biomechanics of endothelial and glial cells and their nuclei, Adv. Sci. 6 (2019) 1–8, https://doi.org/10.1002/advs.201801638.
[25] H. Liu, et al., In situ mechanical characterization of the cell nucleus by atomic force microscopy, ACS Nano 8 (4) (2014) 3821–3828, https://doi.org/10.1021/nn500553z.
[26] H. Xie, J. Song, X. Meng, H. Zhang, In situ quantification of the young's modulus of nuclei in multiple cellular states using a modified fiber probe sensor, IEEE Sensor. J. 19 (8) (2019) 2887–2894, https://doi.org/10.1109/JSEN.2018.2889739.
[27] J. Song, X. Meng, H. Zhang, L. Sun, H. Xie, In situ quantification the complex Poisson's ratio of single cells using a magnetic-drive dynamic atomic force microscopy approach, IEEE Trans. Nanotechnol. 17 (4) (2018) 680–683, https://doi.org/10.1109/TNANO.2018.2799212.
[28] J.S. Milner, M.W. Grol, K.L. Beaucage, S.J. Dixon, D.W. Holdsworth, W. D, Finite-element modelling of viscoelastic cells during high-frequency cyclic strain, J. Funct. Biomater. 3 (2012) 209–224, https://doi.org/10.3390/jfb3010209.
[29] J. Ma, A. Goryaynov, A. Sarma, W. Yang, Self-regulated viscous channel in the nuclear pore complex, Proc. Natl. Acad. Sci. U. S. A. 109 (19) (2012) 7326–7331, https://doi.org/10.1073/pnas.1201724109.
[30] M. Beck, et al., Nuclear Pore complex structure and dynamics revealed by cryoelecton tomography, Science 306 (5700) (2004) 1387–1390, https://doi.org/10.1126/science.1104808.
[31] K.H. Bui, et al., Integrated structural analysis of the human nuclear pore complex scaffold, Cell 155 (6) (2013) 1233–1243, https://doi.org/10.1016/j.cell.2013.10.055.
[32] A. Bestembayeva, et al., Nanoscale stiffness topography reveals structure and mechanics of the transport barrier in intact nuclear pore complexes, Nat. Nanotechnol. 10 (1) (2015) 60–64, https://doi.org/10.1038/nnano.2014.262.
[33] M. Théry, Micropatterning as a tool to decipher cell morphogenesis and functions, J. Cell Sci. 123 (Pt 24) (2010) 4201–4213, https://doi.org/10.1242/jcs.075150.
[34] J.K. Kim, A. Louhghalam, G. Lee, B.W. Schafer, D. Wirtz, D.H. Kim, Nuclear lamin A/C harnesses the perinuclear apical actin cables to protect nuclear morphology, Nat. Commun. 8 (1) (2017) 2123, https://doi.org/10.1038/s41467-017-02217-5.
[35] S. Dupont, et al., Role of YAP/TAZ in mechanotransduction, Nature 474 (7350) (2011) 179–183, https://doi.org/10.1038/nature10137.
[36] E. Sidorenko, K. M, Vartiainen. Nucleoskeletal regulation of transcription: actin on MRTF, Exp. Biol. Med. (Maywood, NJ, U. S.) 244 (15) (2019) 1372–1381, https://doi.org/10.1177/1535370219854669.
[37] A. Das, R.S. Fischer, D. Pan, C.M. Waterman, YAP nuclear localization in the absence of cell-cell contact is mediated by a filamentous actin-dependent, myosin II- and phospho-YAP-independent pathway during extracellular matrix mechanosensing, J. Biol. Chem. 291 (12) (2016) 6096–6110, https://doi.org/10.1074/jbc.M115.708313.
[38] M. Kofler, et al., Mediated nuclear import and export of TAZ and underlying molecular requirements, Nat. Commun. 9 (2018) 4966, https://doi.org/10.1038/s41467-018-07450-0.
[39] B.C. Low, C.Q. Pan, G.V. Shivashankar, A. Bershadsky, M. Sudol, M. Sheetz, YAP/TAZ as mechanosensors and mechanotransducers in regulating organ size and tumor growth, FEBS Lett. 588 (16) (2014) 2663–2670, https://doi.org/10.1016/j.febslet.2014.04.012.
[40] X. Cai, K.C. Wang, Z. Meng, Mechanoregulation of YAP and TAZ in cellular homeostasis and disease progression, Front. Cell Dev. Biol. 9 (2021), https://doi.org/10.3389/fcell.2021.673599.
[41] Christopher S. Chen, et al., Geometric control of cell life and death, Science 5317 (1997) (1997) 1425–1428, https://doi.org/10.1126/science.276.5317.1425, 276.
[42] X. Yao, R. Liu, X. Liang, J. Ding, Critical areas of proliferation of single cells on micropatterned surfaces and corresponding cell type dependence, ACS Appl. Mater. Interfaces 11 (17) (2019) 15366–15380, https://doi.org/10.1021/acsami.9b03780.
[43] W. Kim, Y.S. Cho, X. Wang, O. Park, X. Ma, H. Kim, Y. Yang, Hippo signaling is intrinsically regulated during cell cycle progression by APC/CCdh1, Proc. Natl. Acad. Sci. USA 116 (19) (2019) 9423–9432, https://doi.org/10.1073/pnas.1821370116.
[44] X. Wang, et al., Mechanical stability of the cell nucleus – roles played by the cytoskeleton in nuclear deformation and strain recovery, J. Cell Sci. 131 (13) (2018), jcs209627, https://doi.org/10.1242/jcs.209627.